HHS Public Access

Author manuscript

Am J Reprod Immunol. Author manuscript; available in PMC 2020 December 22.

Published in final edited form as:

Am J Reprod Immunol. 2020 September ; 84(3): e13284. doi:10.1111/aji.13284.

Identification of Unique Clusters of T, Dendritic and Innate Lymphoid Cells in the Peritoneal Fluid of Ovarian Cancer Patients

Jessica Vazquez, **Melina Chavarria**, **Gladys E. Lopez**, **Mildred A. Felder**, **Arvinder Kapur**, **Antonio Romo Chavez**, **Nathan Karst**, **Lisa Barroilhet**, **Manish S. Patankar**[*], **Aleksandar K. Stanic**[*]

Department of Obstetrics and Gynecology, University of Wisconsin-Madison, Madison, WI

Abstract

Problem: We hypothesize that activated peritoneal immune cells can be redirected to target ovarian tumors. Here, we obtain fundamental knowledge of the peritoneal immune environment through deep immunophenotyping of T cells, dendritic cells (DC) and innate lymphoid cells (ILC) of ovarian cancer patients.

Method of study: T cells, DC and ILC from ascites of ovarian cancer patients (n=15) and peripheral blood of post-menopausal healthy donors (n=6) were immunophenotyped on a BD Fortessa cytometer using three panels- each composed of 16 antibodies. The data were analyzed manually and by t-SNE/DensVM. CA125 levels were obtained from patient charts.

Results: We observed decreased $CD3^+$ T cells and a higher proportion of activated $CD4^+$ and effector memory $CD4^+/CD8^+$ T cells, plasmacytoid DC, $CD1c^+$ and $CD141^+$ myeloid DC and $CD56^{Hi}$ NK cells in ascites. t-SNE/DensVM identified eight T cell, 17 DC and 17 ILC clusters that were unique in the ascites compared to controls. Hierarchical clustering of cell frequency distinctly segregated the T cell and ILC clusters from controls. Increased CA125 levels were associated with decreased $CD8^+/CD45RA^+/CD45RO^-/CCR7^-$ T cells.

Conclusions: The identified immune clusters serve as the basis for interrogation of the peritoneal immune environment and the development of novel immunologic modalities against ovarian cancer.

Keywords

Ovarian cancer; Immunophenotyping; Peritoneal fluid; ascites; CD8 T cells; Innate lymphoid cells; dendritic cells; CA125

[*] Correspondence to: A.K. Stanic, Department of Obstetrics and Gynecology, University of Wisconsin-Madison, Perinatal Research, Meriter-park, 202 S. Park Street, Madison, WI 53715, USA, stanickostic@wisc.edu (A.K. Stanic), M.S.Patankar, Department of Obstetrics and Gynecology, University of Wisconsin-Madison, 600 Highland Avenue, H4/654 CSC, Madison, WI-53792, USA, patankar@wisc.edu (M.S.Patankar).

Author contributions

This article was conceptualized by MSP and AKS. JV, MSP and AKS helped major parts of the text. JV, GEL, MF, AK, ARC and LB helped with data and sample acquisition. JV, MC, NK and AKS helped with data analysis and development of figures.

Conflict of interest disclosure statement. All of the co-authors declare that they do not have any relationships that could be construed as resulting in an actual, potential, or perceived conflict of interest with regard to the manuscript being submitted for review.

1 Introduction

High grade serous ovarian cancer (HGSOC) originates in the secretory epithelium of the fallopian tubes or from cortical inclusion cysts in the ovary [1–3]. Metastasis beyond these primary tissues occurs at preferred sites such as the omentum, diaphragm and serosal surfaces within the peritoneal cavity. Proliferation of serous ovarian tumors at these primary and secondary sites is associated with accumulation of ascites in the majority of HGSOC patients [4–6]. Obstruction of the lymphatic ducts is the cause for accumulation of this peritoneal exudate [5,7,8]. Ascites contains acellular factors derived from the tumors, the mesothelial linings as well as the underlying stroma. Cytokines, chemokines, growth factors and other molecules present in the peritoneal fluid and their potential roles in progression and metastasis of ovarian tumors are topics of intense interest [9]. There is also a significant cellular component in ascites that is composed of tumor cells and spheroids, mesothelial cells, stromal cells and immune cells [5,9,10]. In this study, we employ deep immunophenotyping to map the complex immune milieu present in the ascites of HGSOC patients.

There are separate immune cell compartments in most patients with cancer that influence tumor progression. Immune cells in peripheral circulation are most studied for their phenotype as well as their potential roles in developing immunotherapies against HGSOC. The second compartment includes the immune cells infiltrating the solid tumor microenvironment. Supporting an important role for adaptive immune cells, infiltrating CD8+ T cell are positively associated with survival in multiple studies [11,12].

The immune cells in ascites constitute the third most relevant immune compartment in HGSOC. There are limited studies conducted on this compartment even though the immune cells in ascites represent all major subsets of lymphoid and myeloid lineages [13–15]. Ascites immune cells are abundant (typically >100 million per patient; Patankar et al unpublished observations), however, their composition, function and relationship to immune cells infiltrating ovarian tumor stroma remains obscure. The potential for ascites immune cells to target and lyse tumor cells/masses is not well defined. There is evidence that the peritoneal NK cells have suppressed cytolytic activity [16]. In contrast, biology of the peritoneal cytolytic T cells or the drivers of adaptive immunity, dendritic cells is poorly understood. Potential of such an abundant source of readily accessible immune cells for development of immunotherapy regimens is also understudied.

This study was undertaken to develop a foundation for understanding and harnessing the peritoneal immune environment of HGSOC patients. We have employed high-dimensional immunophenotyping to identify common and unique subsets of T cells, dendritic cells and innate lymphoid cells (ILCs). The focus on these three immune groups is due to their established role in immunologic control of tumor progression. Ascites immunome datasets from HGSOC patients were visualized by dimensionality reduction and analyzed by support vector assisted machine learning (densVM) algorithms to identify immune cells and their distribution patterns. These fundamental datasets will serve as the basis for deeper exploration of the peritoneal immune cells and their roles in the biology, patient stratification and therapy of HGSOC.

2 Materials and Methods

2.1 Human Samples

Ascites samples were obtained from patients with ovarian cancer who were recruited at the time of their initial diagnosis (Table 1). None of the patients had been previously treated for their disease at the time of sample collection. All patients signed an informed consent and the studies were approved by the Institutional Review Board of University of Wisconsin-Madison. Ascites samples were heparinized at time of collection and then spun in a Beckman centrifuge at 450xg, 25°C for 20 minutes. The liquid fraction was removed and frozen for later use, while the cell pellet was washed twice in PBS-1%FBS for 10 minutes each at 300xg. Cells were counted and resuspended at appropriate concentrations in FBS-10% DMSO, frozen, and stored in liquid nitrogen until needed.

2.2 Flow Cytometry and Standardization

Isolated mononuclear cells were first labeled with Zombie® NIR stain (BioLegend) according to manufacturer's instructions to discriminate live/dead cells. MCs were then labeled with flourochrome-conjugated monoclonal antibodies, listed in Table 2, as previously described [17]. Samples were then acquired using the LSR Fortessa in a five laser (355nm, 405nm, 488nm, 562nm, 633nm) 20-detector configuration (BD Biosciences).

2.3 Data Analysis

FlowJo v.10 software (FlowJo LLC, Ashland, OR) was used to identify well-characterized populations. Unbiased identification of immune cells was performed using Cytofkit (github.com/JinmiaoChenLab/cytofkit) [18]. Data was pre/post processed as previously described [17]. Statistical significance was determined unpaired t-test, using Prism® v. 8 (GraphPad Software, Inc, La Jolla, CA).

3 Results

3.1 Subset diversity of adaptive T cells in High Grade Serous Ovarian Cancer Ascites

To determine the abundance and functional diversity of $CD4^+$ and $CD8^+$ T cells in High Grade Serous Ovarian Cancer (HGSOC) ascites, we first devised and validated a 16-marker panel (Table 2) to comprehensively phenotype subtypes and effector status using healthy post-menopausal donor peripheral blood mononuclear cells (PBMCs; Supplementary Figure 1). Hereafter, in this study, we employ HD PBMCs as technical reference, and not as a comparator for the phenotype of the immune cells in the ascites of HGSOC patients. Experiments with the HD PBMC samples indicated that relative abundance of $CD3^+$T cells was above 40% in all donors (Supplementary Figure 1G). The $CD4^+$ T cells were more abundant than $CD8^+$ T cells (Supplementary Figure 1H). Higher proportion of the $CD4^+$ T cells were of the T_H2 phenotype and nearly all of the T_{regs} were memory T cells (Supplementary Figure 1 I and J). Additionally, majority of the $CD8^+$ T cells were of the effector memory phenotype (Supplementary Figure 1K). The distribution of the T cell subsets is in accordance with published literature, therefore providing us a general validation of the T cell phenotyping antibody panel and the flow cytometry gating methods used in our analysis.

Of the fifteen HGSOC ascites samples analyzed, three patients had very low levels (<10% relative abundance) of $CD3^+$ T cells (Figure 1C; Supplementary Figure 2). For the majority of the patients (8/15), the relative abundance of the $CD3^+$ T cells was between 25–42% of the total live $CD45^+$ immune cells (Figure 1C). In general, all of the HGSOC ascites samples had comparable proportion of $CD4^+$ and $CD8^+$ T cells (Figure 1D). Further analysis of T cell subsets found a greater proportion were T_H1, T_H2, effector memory, and central memory (Figure 1E), with the majority of T_{regs} in HGSOC ascites being of the memory phenotype (Figure 1F).

Next, we examined the different proportions of $CD8^+$ T cells and found that a large proportion of $CD8^+$ T in HGSOC ascites have an effector memory phenotype (Figure 1G). Overall, these data shows an equal distribution of $CD4^+$ and $CD8^+$ T in HGSOC ascites, with an enrichment of enriched T_H1, T_H2, effector memory, and central memory.

3.2 Dendritic cell distribution in HGSOC Ascites

Because of their importance in bridging the innate and adaptive arms of the immune system, we analyzed antigen presenting cells (APCs) in HGSOC ascites. The antibody panel for analysis of APCs was first tested on HD PBMCs samples (Supplementary Figure 3). A key observation from the HD PBMC samples was that a higher proportion of APCs in HD PBMCs had an HLA-$DR^+CD16^-CD14^+$ phenotype, indicative of macrophages (Supplementary Figure 3). Dendritic cells (DCs), key APCs [19], classically defined by a HLA-$DR^+CD16^-CD14^-$ phenotype (Figure 2A,B) were a higher proportion of APCs in HGSOC ascites (Figure 2E).

Increasing recognition of phenotypically diverse and tissue-specific DC/macrophage subsets led us to first examine the well-defined subtypes within the HLA-$DR^+CD16^-CD14^-$ DC group. Plasmacytoid DCs (pDCs) (Figure 2C) were found to be the more represented subset in HGSOC ascites (Figure 2F). Collectively our data reveal a high proportion of DCs in HGSOC ascites with most being pDCs, and a reduction of $CD14^+$ macrophages.

3.3 Innate lymphoid cells in HGSOC ascites

Innate lymphoid cells (ILCs), described by their lack of antigen-specific receptors, have been found to mirror the T_H cytokine profiles [20]. Use of both surface and intracellular markers (Table 2 and Supplementary Table 1), allowed us to identify lineage negative (CD3, CD14, CD19), $CD34^-CD45^+$ ILCs in HGSOC ascites and HD PBMCs (Figure 3, Supplementary Figure 4). Moreover, we identified conventional $CD56^{Hi}$ and $CD56^{Low}$ natural killer cells (NKs) (Figure 3C), ILC3s ($CD56^+ROR\gamma t^+$), and LTi-like cells ($CD56^-ROR\gamma t^+$) in HGSOC ascites (Figure 3D). NK cells were found in higher proportion in HGSOC ascites compared to ILC3s and LTi-like cells (Figure 3E). A similar pattern was observed in HD PBMCs (Supplementary Figure 4E). Analysis of NK subsets, $CD56^{Bright}$ and $CD56^{Dim}$, found an equal proportion in HGSOC ascites (Figure 3F). Overall, we found a greater proportion of NK cells in HGSOC ascites, with no difference in proportions of ILC3s or LTi-like cells.

3.4 Clustering analysis reveals a unique immunome signature of HGSOC ascites

To test whether HGSOC ascites have a unique immunome, we employed dimensionality reduction to analyze the three data sets. To benchmark our computational analysis and ensure that cluster identification was consistent with published literature, we included the data from HD PBMCs as internal controls. Pre-gated populations of interest from each data set (T cells, DCs, and ILCs) were visualized with t-SNE dimensionality reduction and partitioned with DensVM clustering (Figure 4A). t-SNE/DensVM identified 8 unique clusters within the T cell data set and 17 unique clusters for both the ILC and DC data sets (Figure 4A). In addition, when HD PBMCs and HGSOC ascites samples were visualized separately, distinct cluster distributions were observed for both ILCs and T cells (Figure 4B). This analysis also allowed for unbiased phenotyping of clusters identified by t-SNE/DensVM (Supplementary Figure 5, Supplementary Table 1).

In order to assess the variation in immune cell clusters among patients, we conducted hierarchical clustering based on cell frequency distribution. First, T cell cluster distribution showed low degree of segregation between the HGSOC ascites samples (Figure 5A). The frequencies of clusters 2 and 4 were generally uniformly higher in all of the HGSOC patients (Figure 5A). In contrast, frequencies of clusters 7 and 8 were lower in the majority of the HGSOC ascites samples (Figure 5A).

Cluster distribution from the DC dataset revealed two major groupings of the HGSOC ascites samples (Figure 5B). Two clusters (#1 and #14) that were enriched in HGSOC ascites samples, highlighting populations ($CD8\alpha^-$, $CD11b^-$ dendritic cells and $CD11b^+$ dendritic cells, respectively) that were not captured in our manual analysis (Figure 2).

Similarly, to T cell clustering results, ILCs cluster distribution showed lower degree of distinction between the HGSOC ascites samples (Figure 5C), with segregation of HGSOC ascites from HD samples. Clusters #1, 2, 3, and 13 were all elevated in HGSOC ascites samples. Clusters #1–3 were found to be tissue-resident-like natural killer cells (Supplementary Table 1). Interestingly, clusters #9, 11, 14, and 17 (all fitting the phenotype of cNKs) were elevated in HD PBMC samples, in agreement with our manual data analysis (Supplementary Figure 4F).

3.5 Correlation of immune cell subsets from ascites with serum CA125 levels.

The serum levels of the biomarker CA125 typically correspond to ovarian cancer disease progression. We reasoned that since an increase in serum CA125 is associated with higher tumor burden, there would likely be a correlation between the levels of serum CA125 and specific immune cell types in the ascites. While the study was not significantly powered to directly correlated CA125 levels with majority of the clusters identified through our deep immunophenotyping, the most significant correlation was observed with the $CD8^+$ T effector cells defined by Cluster #5 (Figure 6). This cluster is defined as T cells that are $CD8^+/CD45RA^+/CD45RO^-/CCR7^-$. Elevated serum CA125 levels were highly correlated with decreased proportion of Cluster #5 (Figure 6).

4 Discussion

The results of this study provide a framework for deep immunophenotyping to identify unique subsets of immune cells present in the peritoneal fluid of HGSOC patients. In this study, we have specifically characterized T cells, dendritic cells and ILC subsets from the ascites of HGSOC patients. Immune cells in ascites of ovarian cancer patients have been previously identified and characterized using conventional flow cytometry methods [21–24]. These previous approaches require cell labeling and analysis in batches as only limited number of fluorophores were included in each experiment. Our deep immunophenotyping approach has allowed us to characterize multiple subsets of T cells, DCs and ILCs in a single experiment. This approach not only provides more clarity of the different subsets of immune cells but also allows us to capture this data using minimum amount of biological samples. The T and DC subsets identified in our studies in addition to the information provided in previous studies is providing important insights into the immune environment in the peritoneum of ovarian cancer patients. To our knowledge, our study is the first to characterize the peritoneal ILCs from this patient population.

Manual analysis of the flow cytometry data suggests that the ascites immune cells have a higher proportion of activated $CD4^+$ and effector memory (both $CD4^+$ and $CD8^+$) T cells. An increase in DCs and the DC subsets (pDCs and $CD1c^+$ and $CD141^+$ mDCs) is also observed in the HGSOC ascites.

Another major finding from the manual analysis of the flow cytometry results was the significant increase in proportion of the $CD56^{bright}$t NK cells. This population of NK cells is compromised in cytolysing cancer targets but is more efficient in producing cytokines. To the contrary, the $CD16^+$ NK cell population that is classically associated with cytotoxic responses was significantly reduced in the HGSOC ascites. This observation confirms our previous studies where we demonstrated that MUC16, a mucin highly expressed by ovarian tumors downregulates CD16 on NK cells and suppresses their cytolytic function [13,25–27]. In this context, it is important to note that the serum levels of CA125, a repeating peptide epitope present in MUC16 [26,28,29], negatively correlate with the proportion of CD8 effector cells in the peritoneal environment. This correlation may result from the fact that higher levels of serum CA125 reflect a more advanced state of the cancer and hence a more immunocompromised peritoneal environment. It will also be important to determine if similar to the immunosuppressive effects of MUC16 on NK cells, this mucin also plays a role in suppressing cytolytic T cell responses. Our demonstration that MUC16 is a ligand of the glycoimmune checkpoint receptor Siglec-9, an inhibitory ITIM-containing receptor that negatively regulates innate and adaptive immune cells is significant in this context because increase expression of Siglec-9 has been detected on T cells in the ovarian cancer microenvironment [25,30–32].

The multiparameter deep-immunophenotyping data afford us the opportunity to classify multiple subsets of the immune cells from ascites and conduct hierarchical clustering. Eight unique clusters of T cells and 17 individual clusters of DC and ILCs were identified based on the level of expression of the cell surface markers that are the hallmarks of each cluster. t-SNE mapping of the cluster frequencies showed a shared hierarchy of the T cell and ILCs of

the ascites immune cells. The shared hierarchy of the peritoneal immune cells among HGSOC patients suggest that the immune cells are under the influence of common activating and suppressive factors that influence the phenotype of the T cells and ILCs. This finding indicates that the phenotypes identified in in this study are representative of a significant proportion of HGSOC patients. In the future, it will be important to determine if there is an association between the proportions of the peritoneal immune cell subsets with the mutations found in the serous ovarian tumors.

A limitation of our study is that the phenome of the immune cells from the HGSOC ascites fluid was compared with that of the T cells, DC and ILC from the peripheral blood of healthy donors. We are in the process of obtaining a bank of matched immune cell samples from the ascites and peripheral blood of HGSOC patients. Future studies will compare the phenome of the immune cells from these matching set of immune cell samples. However, it should be noted that in our previous studies conducted with a limited panels of antibodies, we did not observe major differences in the phenotypes of T cells, B cells and NK cells from the peripheral blood of HGSOC patients and healthy donors [13]. Therefore, we expect that similar to the immune cells from healthy donors, the peripheral T cells and ILCs of HGSOC patients will show a hierarchy that is distinct than the immune cells from the ascites.

The deep immunophenotyping results provide important insights into the peritoneal immune environment of HGSOC patients. It is expected that the results from these studies can be used to manipulate the peritoneal immune cells and redirect them to target the metastasized ovarian tumors. Immunotherapeutic agents that activate the peritoneal immune cells and block the immunosuppressive mechanisms can be used to develop robust immunologic responses against HGSOC.

We have conducted a detailed analysis of the T cells, DCs and ILCs from the peritoneal fluid of HGSOC patients. Through deep immunophenotyping we have identified unique clusters of the peritoneal immune cells. The T cells and ILC from HGSOC ascites hierarchically cluster together as compared to the immune cell subsets from the peripheral blood of healthy donors. Since the ascites samples were obtained from HGSOC patients prior to their debulking surgery and chemotherapy, the phenotypes identified in this study are the result of the influence of factors produced in the tumor microenvironment. Therefore, these phenotypes should be considered as the baseline for peritoneal immune cells in HGSOC patients. These baseline phenotypes can be compared to those identified in future studies where the HGSOC patients are treated with immunotherapies. Such comparisons will provide an assessment of the functional capacity of the peritoneal immune cells in response to the treatment modalities. Additionally, the deep phenotyping datasets can also be used to identify and expand immune cell subsets that can most effectively be used to target peritoneal ovarian tumors.

Supplementary Material

Refer to Web version on PubMed Central for supplementary material.

Acknowledgements

This research was supported by the bridge grant (ID: 598088) from the Rivkin Center for Ovarian Cancer to MSP and intramural research funds provided by the Department of Obstetrics and Gynecology to LB, MSP and AKS. J.V. was supported by NIH TEAM-Science (R25 GM083252) and UW SciMed GRS Fellowship. M.C. was supported by WISE Summer Research Grant. A.K.S. was supported by NIH/NICHD Reproductive Scientist Development Program (5K 12HD000849-28), March of Dimes Basil O'Connor Award (5-FY18-541), and Burroughs Wellcome Fund (1019835). Studies were supported by University of Wisconsin Carbone Cancer Center Support Grant (P30 CA014520). The BD Fortessa analytical cytometer used in the studies was supported by a special instrumentation grant (1S100OD018202-01). D. Sheerar and R. Sheridan from UWCCC Flow lab are acknowledged for technical support.

References

1. Labidi-Galy SI, Papp E, Hallberg D, et al. High grade serous ovarian carcinomas originate in the fallopian tube. Nat Commun. 2017;8(1):1093. [PubMed: 29061967]
2. Visvanathan K, Shaw P, May BJ, et al. Fallopian Tube Lesions in Women at High Risk for Ovarian Cancer: A Multicenter Study. Cancer Prev Res (Phila). 2018;11(11):697–706. [PubMed: 30232083]
3. Kurman RJ, Shih Ie M. Molecular pathogenesis and extraovarian origin of epithelial ovarian cancer--shifting the paradigm. Hum Pathol. 2011;42(7):918–931. [PubMed: 21683865]
4. Ahmed N, Stenvers KL. Getting to know ovarian cancer ascites: opportunities for targeted therapy-based translational research. Frontiers in oncology. 2013;3:256–256. [PubMed: 24093089]
5. Kipps E, Tan DS, Kaye SB. Meeting the challenge of ascites in ovarian cancer: new avenues for therapy and research. Nat Rev Cancer. 2013;13(4):273–282. [PubMed: 23426401]
6. Ayantunde AA, Parsons SL. Pattern and prognostic factors in patients with malignant ascites: a retrospective study. Ann Oncol. 2007;18(5):945–949. [PubMed: 17298959]
7. Holm-Nielsen P Pathogenesis of ascites in peritoneal carcinomatosis. Acta Pathol Microbiol Scand. 1953;33(1):10–21. [PubMed: 13113944]
8. Feldman GB, Knapp RC, Order SE, Hellman S. The role of lymphatic obstruction in the formation of ascites in a murine ovarian carcinoma. Cancer Res. 1972;32(8):1663–1666. [PubMed: 5044130]
9. Milliken D, Scotton C, Raju S, Balkwill F, Wilson J. Analysis of chemokines and chemokine receptor expression in ovarian cancer ascites. Clin Cancer Res. 2002;8(4):1108–1114. [PubMed: 11948121]
10. Sheid B Angiogenic effects of macrophages isolated from ascitic fluid aspirated from women with advanced ovarian cancer. Cancer Lett. 1992;62(2):153–158. [PubMed: 1371714]
11. Preston CC, Maurer MJ, Oberg AL, et al. The ratios of CD8+ T cells to CD4+CD25+ FOXP3+ and FOXP3- T cells correlate with poor clinical outcome in human serous ovarian cancer. PLoS One. 2013;8(11):e80063. [PubMed: 24244610]
12. Hamanishi J, Mandai M, Iwasaki M, et al. Programmed cell death 1 ligand 1 and tumor-infiltrating CD8+ T lymphocytes are prognostic factors of human ovarian cancer. Proc Natl Acad Sci U S A. 2007;104(9):3360–3365. [PubMed: 17360651]
13. Belisle JA, Gubbels JA, Raphael CA, et al. Peritoneal natural killer cells from epithelial ovarian cancer patients show an altered phenotype and bind to the tumour marker MUC16 (CA125). Immunology. 2007;122(3):418–429. [PubMed: 17617155]
14. Hashimoto K, Honda K, Matsui H, Nagashima Y, Oda H. Flow Cytometric Analysis of Ovarian Cancer Ascites: Response of Mesothelial Cells and Macrophages to Cancer. Anticancer Res. 2016;36(7):3579–3584. [PubMed: 27354626]
15. Gordon IO, Freedman RS. Defective antitumor function of monocyte-derived macrophages from epithelial ovarian cancer patients. Clin Cancer Res. 2006;12(5):1515–1524. [PubMed: 16533776]
16. Connor JP, Felder M, Hank J, et al. Ex vivo evaluation of anti-EpCAM immunocytokine huKS-IL2 in ovarian cancer. J Immunother. 2004;27(3):211–219. [PubMed: 15076138]
17. Vazquez J, Chavarria M, Li Y, Lopez GE, Stanic AK. Computational flow cytometry analysis reveals a unique immune signature of the human maternal-fetal interface. Am J Reprod Immunol. 2018;79(1).

18. Wong MT, Chen J, Narayanan S, et al. Mapping the Diversity of Follicular Helper T Cells in Human Blood and Tonsils Using High-Dimensional Mass Cytometry Analysis. Cell Rep. 2015;11(11):1822–1833. [PubMed: 26074076]
19. Banchereau J, Steinman RM. Dendritic cells and the control of immunity. Nature. 1998;392(6673):245–252. [PubMed: 9521319]
20. Tait Wojno ED, Artis D. Emerging concepts and future challenges in innate lymphoid cell biology. J Exp Med. 2016;213(11):2229–2248. [PubMed: 27811053]
21. Bamias A, Tsiatas ML, Kafantari E, et al. Significant differences of lymphocytes isolated from ascites of patients with ovarian cancer compared to blood and tumor lymphocytes. Association of CD3+CD56+ cells with platinum resistance. Gynecol Oncol. 2007;106(1):75–81. [PubMed: 17433425]
22. Giuntoli RL 2nd, Webb TJ, Zoso A, et al. Ovarian cancer-associated ascites demonstrates altered immune environment: implications for antitumor immunity. Anticancer Res. 2009;29(8):2875–2884. [PubMed: 19661290]
23. Wefers C, Duiveman-de Boer T, Yigit R, et al. Survival of Ovarian Cancer Patients Is Independent of the Presence of DC and T Cell Subsets in Ascites. Front Immunol. 2018;9:3156. [PubMed: 30687337]
24. Lieber S, Reinartz S, Raifer H, et al. Prognosis of ovarian cancer is associated with effector memory CD8(+) T cell accumulation in ascites, CXCL9 levels and activation-triggered signal transduction in T cells. Oncoimmunology. 2018;7(5):e1424672. [PubMed: 29721385]
25. Belisle JA, Horibata S, Jennifer GA, et al. Identification of Siglec-9 as the receptor for MUC16 on human NK cells, B cells, and monocytes. Mol Cancer. 2010;9:118. [PubMed: 20497550]
26. Felder M, Kapur A, Gonzalez-Bosquet J, et al. MUC16 (CA125): tumor biomarker to cancer therapy, a work in progress. Mol Cancer. 2014;13:129. [PubMed: 24886523]
27. Patankar MS, Jing Y, Morrison JC, et al. Potent suppression of natural killer cell response mediated by the ovarian tumor marker CA125. Gynecol Oncol. 2005;99(3):704–713. [PubMed: 16126266]
28. O'Brien TJ, Beard JB, Underwood LJ, Dennis RA, Santin AD, York L. The CA 125 gene: an extracellular superstructure dominated by repeat sequences. Tumour Biol. 2001;22(6):348–366. [PubMed: 11786729]
29. Yin BW, Lloyd KO. Molecular cloning of the CA125 ovarian cancer antigen: identification as a new mucin, MUC16. J Biol Chem. 2001;276(29):27371–27375. [PubMed: 11369781]
30. Stanczak MA, Siddiqui SS, Trefny MP, et al. Self-associated molecular patterns mediate cancer immune evasion by engaging Siglecs on T cells. J Clin Invest. 2018;128(11):4912–4923. [PubMed: 30130255]
31. Ikehara Y, Ikehara SK, Paulson JC. Negative regulation of T cell receptor signaling by Siglec-7 (p70/AIRM) and Siglec-9. J Biol Chem. 2004;279(41):43117–43125. [PubMed: 15292262]
32. Avril T, Floyd H, Lopez F, Vivier E, Crocker PR. The membrane-proximal immunoreceptor tyrosine-based inhibitory motif is critical for the inhibitory signaling mediated by Siglecs-7 and −9, CD33-related Siglecs expressed on human monocytes and NK cells. J Immunol. 2004;173(11):6841–6849. [PubMed: 15557178]

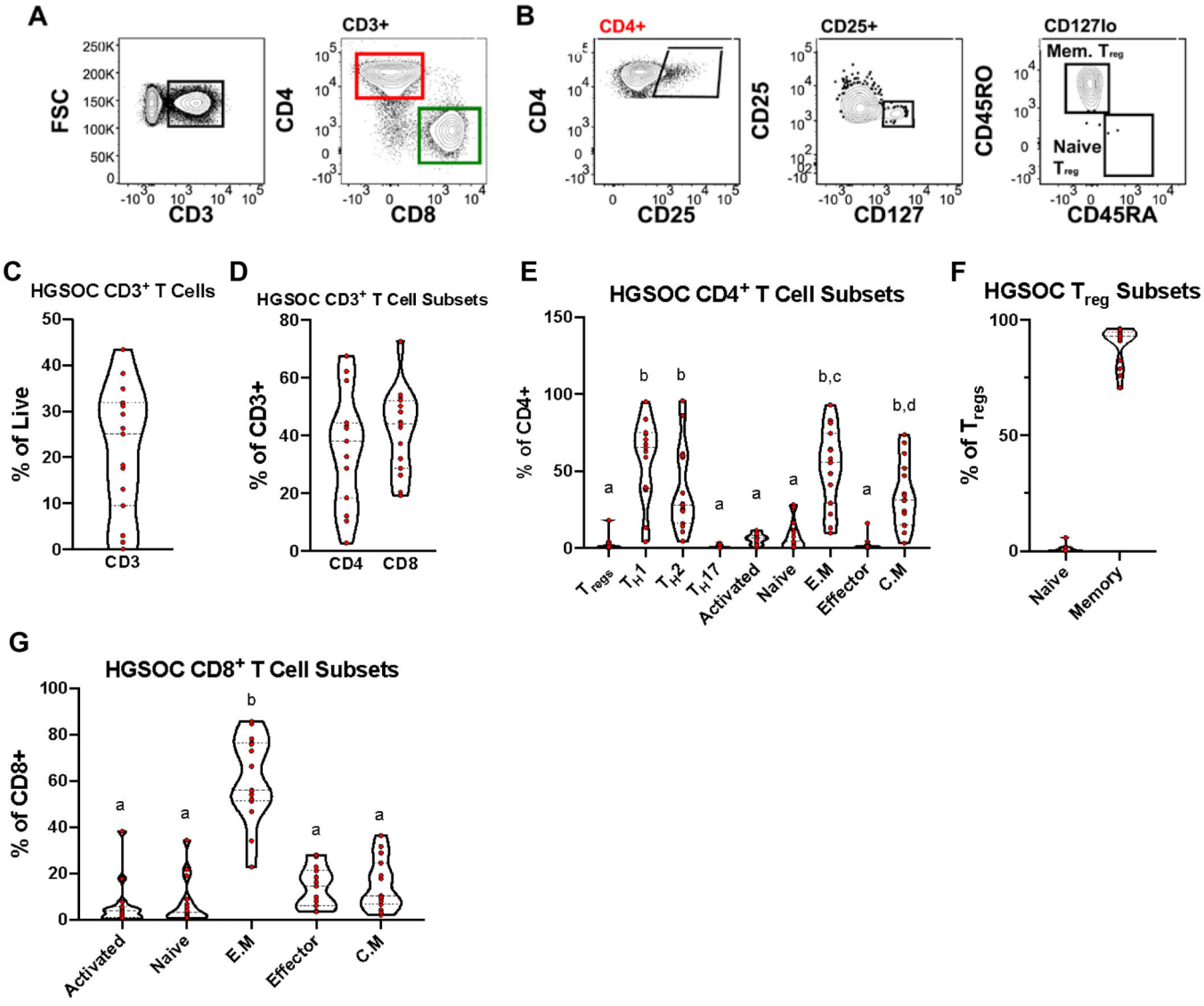

Figure 1.

T Cells Identified in High Grade Serous Ovarian Cancer Ascites Mononuclear cells isolated from High Grade Serous Ovarian Cancer (HGSOC) ascites samples were stained with T cell specific markers. (A) Representative gating scheme identifying $CD3^+$ T cells (left) and CD4/CD8 subsets (right) in HGSOC ascites. (B) Representative gating scheme identifying regulatory T cells (T_{reg}) and T_{reg} subsets. (C) Proportion of $CD3^+$ T cells in HGSOC from total live cells. (D) Proportion of $CD4^+$ and $CD8^+$ from $CD3^+$ T cells. (E) Proportion of $CD4^+$ T cell subsets. (F) Proportion of T_{reg} subsets. (G) Proportion $CD8^+$ T cells subsets. Data represented as max/min, median, and 25^{th} and 75^{th} percentiles. Statistical significance was determined by ANOVA followed by Tukey test and are demonstrated by letters, with different letters indicating statistical differences within a subset (<0.05). HGSOC, n = 15.

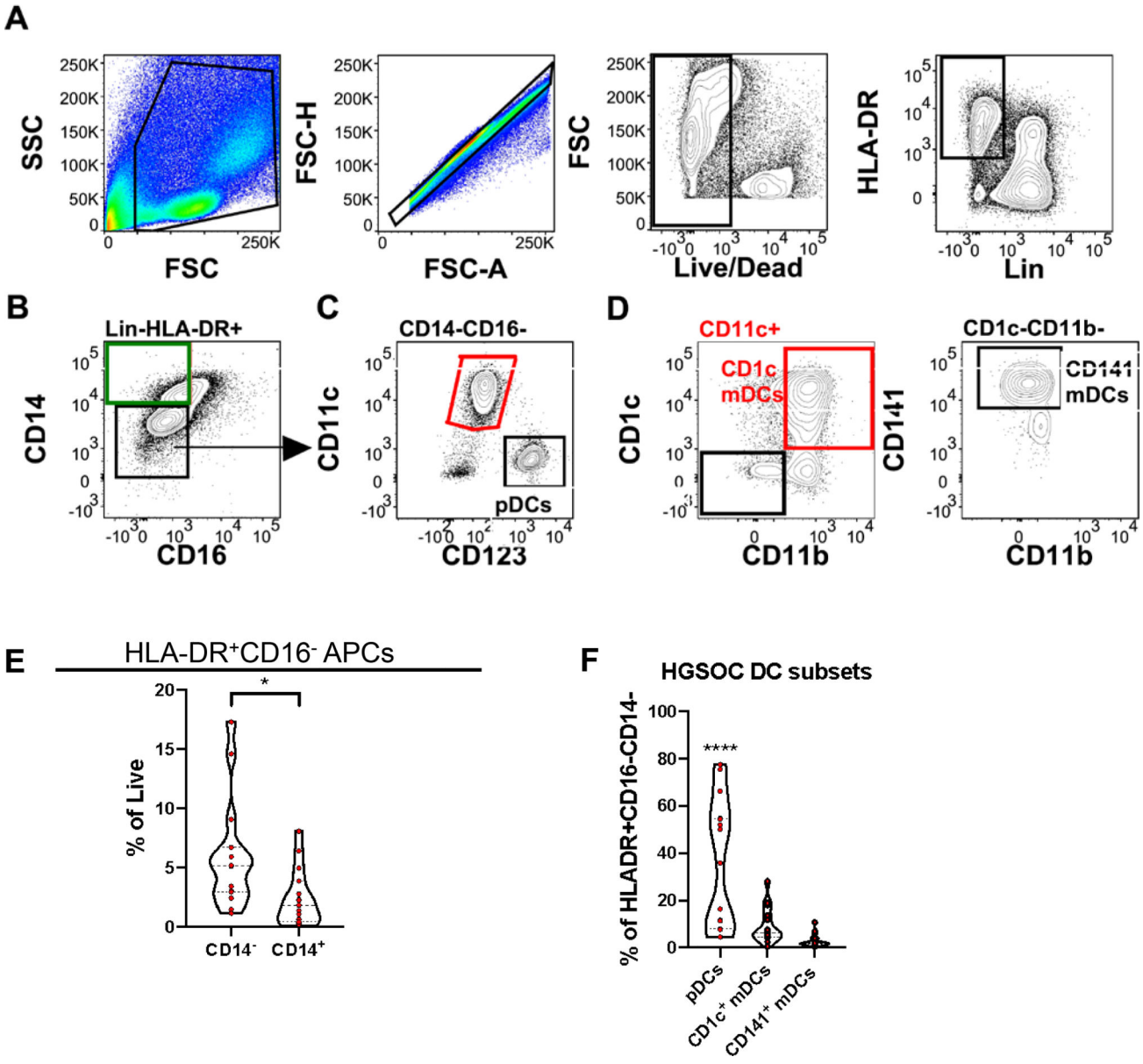

Figure 2.

Antigen presenting cells identified in HGSOC ascites. Mononuclear cells isolated from HGSOC ascites samples were stained with antigen presenting cell (APCs) lineage defining markers. (A) Representative gating scheme identifying Lin(CD3,19,56)$^{-}$HLA-DR^{+} cells in HGSOC ascites samples. (B) Representative gating scheme identifying dendritic cells (DCs; HLA-DR^{+}CD14^{-}CD16^{-}) and macrophages (HLA-DR^{+}CD14^{+}CD16^{-}). (C) Representative gating scheme identifying myeloid (mDCs) and plamacytoid dendritic cells (pDCs). (D) Representative gating scheme identifying CD1c^{+} mDCs (left) and CD141^{+} mDCs (right). (E) Proportion of HLA-DR^{+}CD16^{-} CD14^{-} and CD14^{+} APCs from total live cells. (F) Proportion of pDCs, CD1c mDCs, and CD141 mDCs from total DCs. Data represented as max/min, median, and 25th and 75th percentiles. Statistical significance was determined by ANOVA followed by Tukey test. *p < 0.05, ****p < 0.0001. HGSOC, n = 15.

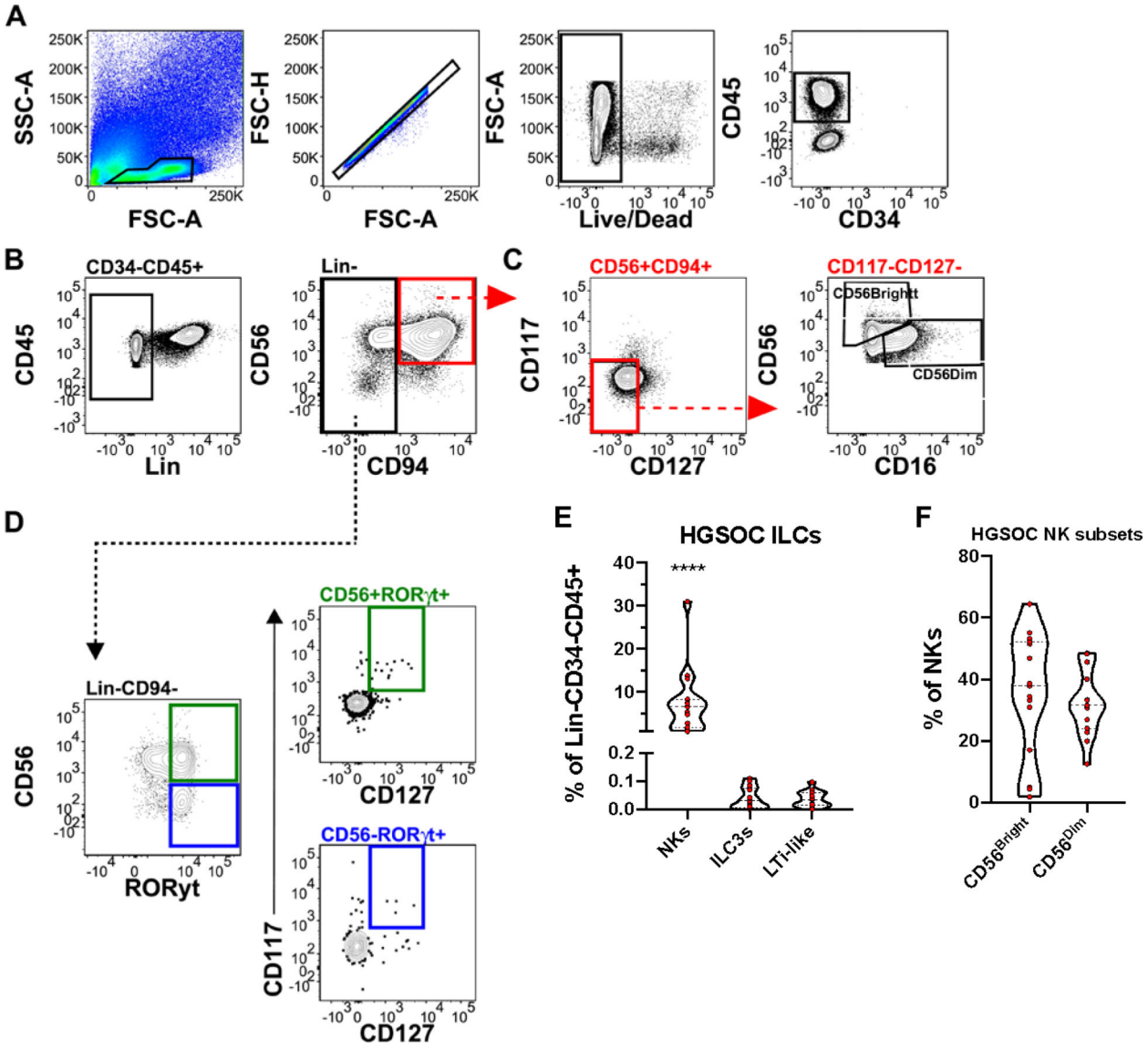

Figure 3.

Innate Lymphoid Cells Identified in HGSOC Ascites. Mononuclear cells isolated from HGSOC ascites samples were stained with innate lymphoid cells (ILC) lineage defining markers. (A) Representative gating scheme identifying $CD34^{-}CD45^{+}$ cells in HGSOC ascites samples. (B) Representative gating scheme identifying Lin (CD3, 14, 19) negative ILCs. (C) Representative gating scheme identifying natural killer cells (NKs) and NK subsets, $CD56^{Bright/Dim}$. (D) Representative gating scheme identifying ILC3s (top) and Lti-like (bottom) cells. (E) Proportion of NKs, ILC3s, and LTi-like cells in HGSOC ascites from total lineage negative lymphoid cells (F) Proportion of NK cells subsets from total NK cells. Data represented as max/min, median, and 25^{th} and 75^{th} percentiles. Statistical significance was determined by ANOVA followed by Tukey test. ****$p < 0.0001$. HGSOC, n = 15.

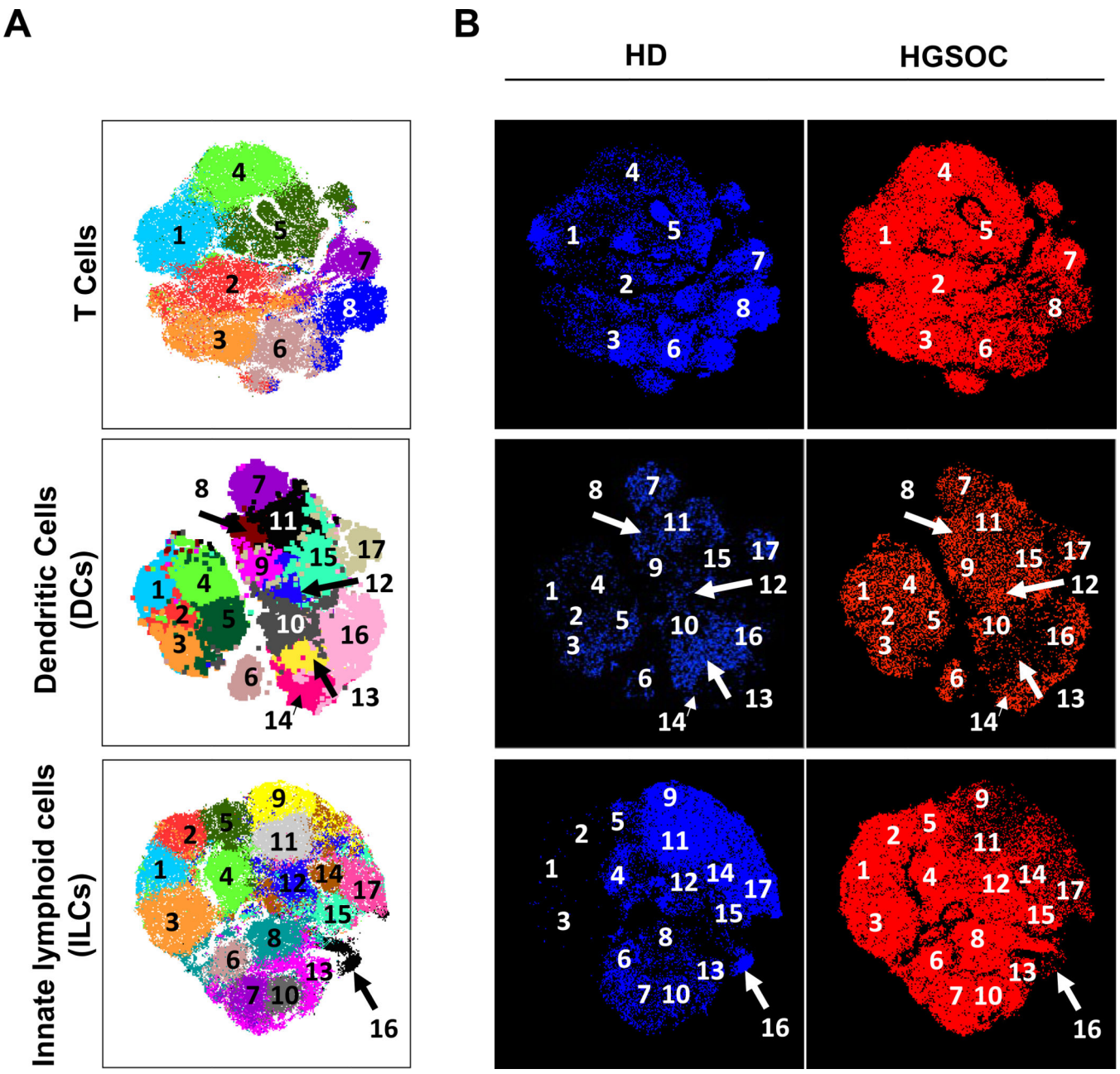

Figure 4.

Subset diversity in HGSOC ascites as revealed dimensionality reduction visualization. (A) t-SNE map generated for pre-gated $CD3^+$ T cells (top), $Lin^-CD14^-CD16^-HLADR^+$ DCs (middle), and $Lin^-CD34^-CD45^+$ ILCs (bottom). (B) Separate HD and HGSOC visualized using t-SNE maps generated from merged data set for T cells (top), DCs (middle), and ILCs (bottom).

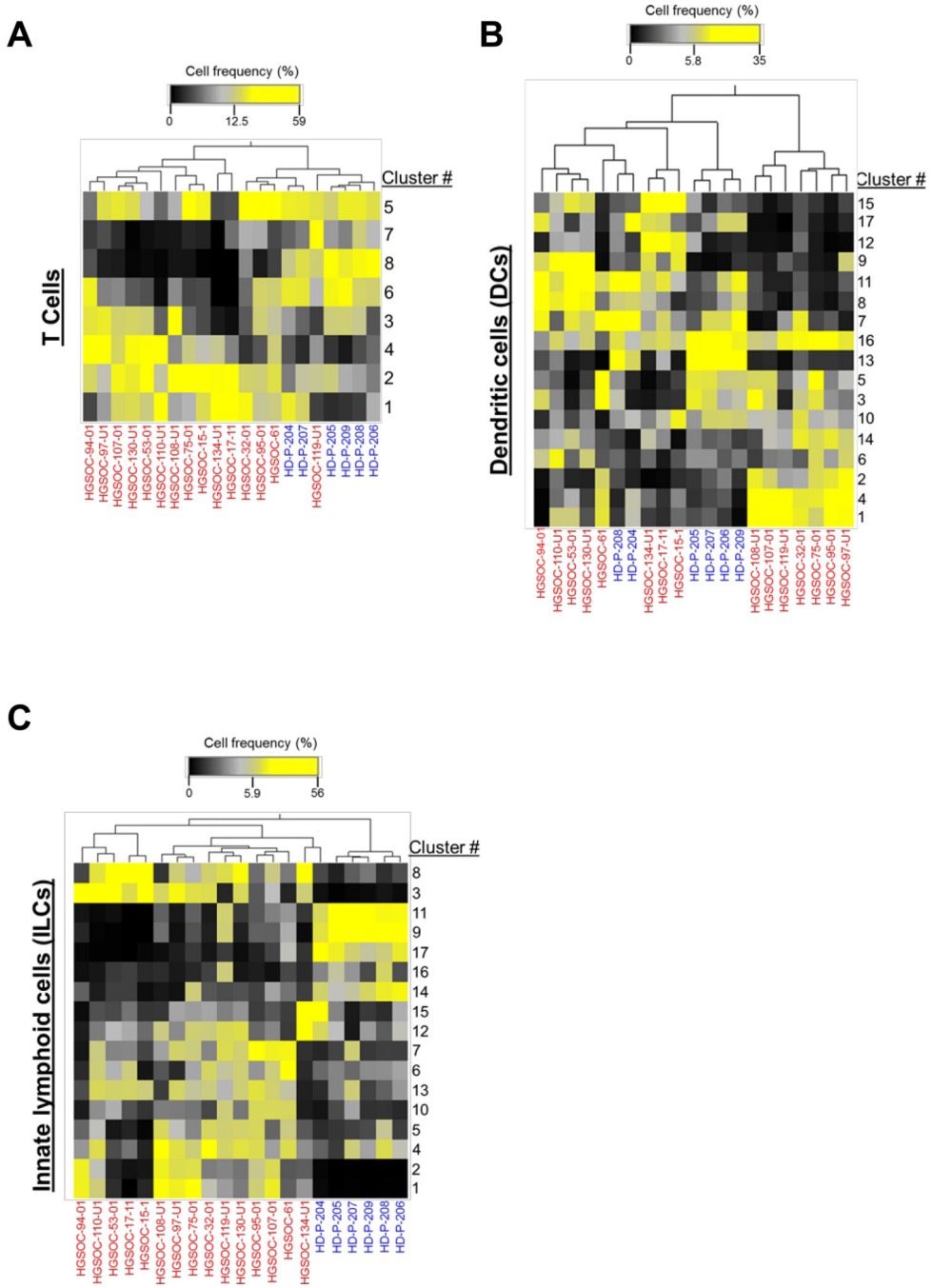

Figure 5.

Cluster distribution analysis reveals unique HGSOC immune signature. Hierarchical clustering of cluster frequencies within T cells, DCs, and ILCs from HGSOC (red) and HD (blue).

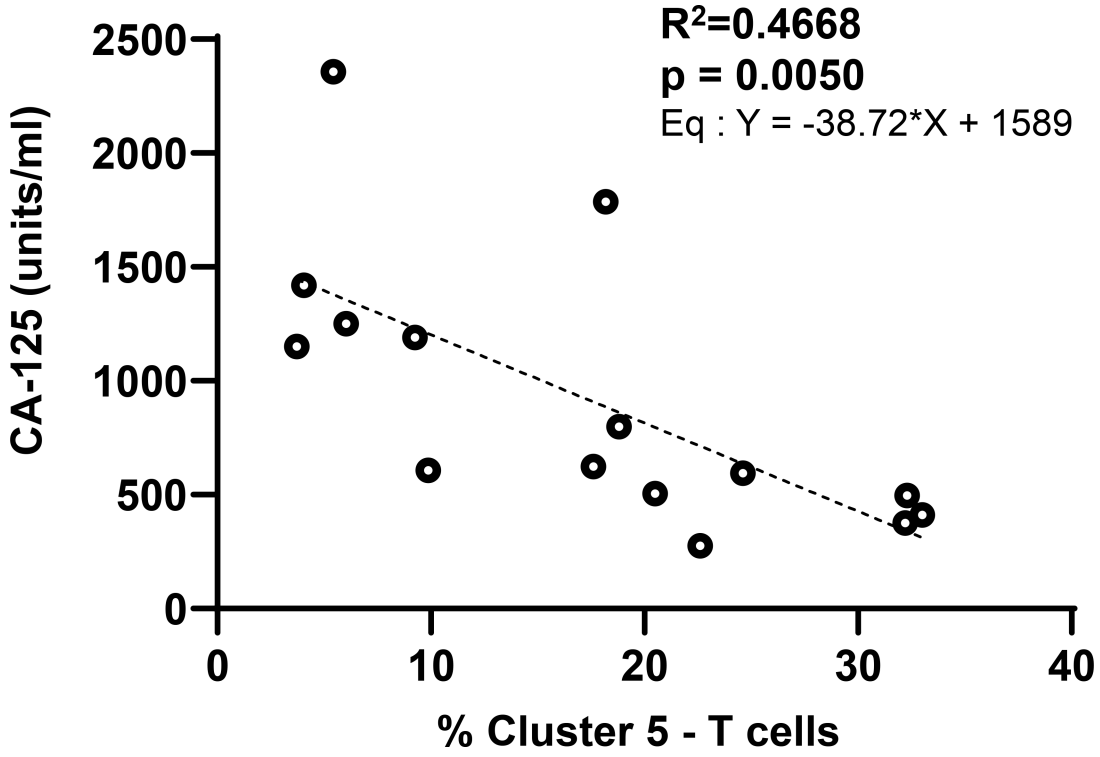

Figure 6.

Initial CA-125 level is inversely correlated to proportion of ascites CD8 effector cells. Linear regression plot of first CA-125 level against proportion of cluster 5 (CD8+ CD45RA + CD45RO- CCR7-CD62L-) T cells.

Table 1.

Demographic and diagnosis information of ovarian cancer patients included in this study

Patient Number	Age at Diagnosis	Diagnosis	Stage	Grade, cell type	CA-125 at Diagnosis
OSC94	73	Ovarian cancer	IIIC	High grade papillary serous	1252
OSC97	69	Ovarian cancer	IV	High grade papillary serous	608
OSC15	55	Ovarian cancer	IIIC	High grade papillary serous	595
OSC61	48	Ovarian cancer	IIIC	Low grade papillary serous	411
OSC32	56	Ovarian cancer	IIIC	Poorly differentiated adenocarcinoma of the ovary	496
OSC108	69	Ovarian cancer	IIIC	High grade papillary serous	1150
OSC53	61	Ovarian cancer	IIIC	High grade papillary serous	624
OSC17	77	Ovarian cancer	IIIC	High grade papillary serous	506
OSC119	51	Fallopian tube cancer	IIIC	High grade papillary serous	376
OSC110	66	Ovarian cancer	IIIC	High grade papillary serous	2357
OSC95	44	Ovarian cancer	IIIC	Papillary serous	1787
OSC130	62	Ovarian cancer	IV	Poorly differentiated neuroendocrine, high-grade serous and endometrioid	275
OSC107	57	Fallopian tube cancer	IIIC	High grade serous adenocarcinoma	798
OSC75	57	Ovarian cancer	IIIC	High grade serous	1191
OSC134	71	Ovarian cancer	IIIC	High grade serous	1419

Table 2

Antibodies used for flow cytometry analysis.

Marker	Clone	Fluorochrome	Supplier
CCR4	1G1	PerCP-Cy5.5	BD Bioscience
CCR6	11A9	BUV496	BD Bioscience
CCR7	G043H7	Alexa647	BioLegend
CD117	104D2	BB515	BD Bioscience
CD11b	ICRF44	BV605	BD Bioscience
CD11c	B-ly6	BB515	BD Bioscience
CD123	7G3	BUV395	BD Bioscience
CD127	A019D5	BV785	BioLegend
CD14	MOP9	BV510	BD Bioscience
CD141	1A4	APC	BD Bioscience
CD16	3G8	BUV496	BD Bioscience
CD161	DX12	BV650	BD Bioscience
CD19	SJ25C1	PE-Cy7	BD Bioscience
CD19	SJ25C1	BV510	BD Bioscience
CD1c	L161	PE-Dazzle594	BioLegend
CD209	DCN46	PerCP-Cy5.5	BD Bioscience
CD25	2A3	BB515	BD Bioscience
CD27	M-T271	BV421	BD Bioscience
CD3	SK7	PE-Cy7	BD Bioscience
CD3	UCHT1	BV510	BD Bioscience
CD33	WM53	PE	BioLegend
CD335 (NKp46)	9E2/NKp46	PE	BD Bioscience
CD34	581	PE-Cy5	BD Bioscience
CD4	SK3	BV510	BD Bioscience
CD45	2D1	Alexa700	BioLegend
CD45RA	HI100	Alexa700	BD Bioscience
CD45RO	UCHL1	PE	BioLegend
CD49a	TS2/7	PE-Vio770	Miltenyi
CD56	NCAM16.2	BV421	BD Bioscience
CD56	B156	PE-Cy7	BD Bioscience
CD62L	Dreg-56	PE-CF594	BD Bioscience
CD8	SK1	BV605	BD Bioscience
CD8	RPA-T8	BV421	BD Bioscience
CD80	L307.4	Alexa700	BD Bioscience
CD94	HP-3D9	PerCP-Cy5.5	BD Bioscience
CXCR3	AC6/CXCR3	PE-Cy5	BD Bioscience
CXCR4	12G5	BUV395	BD Bioscience
Eomes	WM53	PE-eFluor610	eBioscience
HLA-DR	G46–6	BV786	BD Bioscience

Marker	Clone	Fluorochrome	Supplier
HLA-DR	G46–6	BUV395	BD Bioscience
RORγt	AFKJS-9	APC	eBioscience
T-bet	O4–46	BV650	BD Bioscience